Phase Transition in Force during Ramp Stretches of Skeletal Muscle

Elise Burmeister Getz,* Roger Cooke,*# and Steven L. Lehman#§

*Department of Biochemistry and Biophysics, and the Cardiovascular Research Institute, University of California, San Francisco, California 94143; #UCSF/UCB Bioengineering Graduate Group, University of California, San Francisco, California 94143, and Berkeley, California 94720; and §Department of Integrative Biology, University of California, Berkeley, California 94720 USA

ABSTRACT   Active glycerinated rabbit psoas fibers were stretched at constant velocity (0.1–3.0 lengths/s) under sarcomere length control. As observed by previous investigators, force rose in two phases: an initial rapid increase over a small stretch (phase I), and a slower, more modest rise over the remainder of the stretch (phase II). The transition between the two phases occurred at a critical stretch (L_C) of 7.7 ± 0.1 nm/half-sarcomere that is independent of velocity. The force at critical stretch (P_C) increased with velocity up to 1 length/s, then was constant at 3.26 ± 0.06 times isometric force. The decay of the force response to a small step stretch was much faster during stretch than in isometric fibers. The addition of 3 mM vanadate reduced isometric tension to 0.08 ± 0.01 times control isometric tension (P_0), but only reduced P_C to 0.82 ± 0.06 times P_0, demonstrating that prepowerstroke states contribute to force rise during stretch. The data can be explained by a model in which actin-attached cross-bridges in a prepowerstroke state are stretched into regions of high force and detach very rapidly when stretched beyond this region. The prepowerstroke state acts as a mechanical rectifier, producing large forces during stretch but small forces during shortening.

INTRODUCTION

When muscle fibers, either activated or at rest, are subjected to constant velocity stretch, force rises in two phases. The first phase is very steep, with force in an active fiber increasing to at least twice the isometric tension (P_0) over an extension of only a few nanometers per half-sarcomere (nm/hs). The second is much less steep, with force rising less than $1P_0$ over an extension of tens of nanometers per half-sarcomere. The transition between the two phases of force rise occurs after some critical amount of stretch. The critical amount of stretch has been interpreted as a critical strain of each cross-bridge (Hill, 1968; Flitney and Hirst, 1978; Edman et al., 1978; Lombardi and Piazzesi, 1990; Stienen et al., 1992), beyond which it is obliged to detach from actin. Mechanically detached cross-bridges must also reattach rapidly, for force to be maintained in the second phase (Hill, 1968; Flitney and Hirst, 1978; Güth and Kuhn, 1978; Griffiths et al., 1980). Colomo et al. (1989b) also noted that the detachment rate must be small over some range of cross-bridge strain to keep that range populated at high velocities of stretch.

When these ideas are implemented in models of cross-bridge mechanics, a difficulty becomes apparent: the rapid attachment necessary to maintain force during stretch at high velocities is, in the simplest models, inconsistent with the decline in cross-bridge number during shortening. Harry et al. (1990) varied the detachment rate transition function $g(x)$ of the model put forward by A. F. Huxley in 1957, in

an attempt to fit both lengthening and shortening data. They found that force during stretch in this model was maintained by cross-bridges extended to extreme lengths, exceeding the assumed repeat distance between actin sites. The introduction of a maximum allowable cross-bridge strain implied that force would decrease as stretch velocity increased. Lombardi and Piazzesi (1990); Piazzesi et al. (1992, 1995) proposed models that solved this problem. Rapid reattachment of mechanically detached cross-bridges populates force-producing states. They hypothesize a special detached state for these cross-bridges, which is only populated during stretch.

We present a new model that explains the mechanics of stretched fibers, which is derived from identified biochemical states and is compatible with current structural models of the contractile proteins and with shortening mechanics. In this model most of the force during stretch is produced by cross-bridges in a prepowerstroke state that acts as a mechanical rectifier, producing large forces during stretch but small forces during shortening. Cross-bridges in this state are stretched to produce large forces, detach at a critical strain, then reattach rapidly. The same rapid kinetics apply during shortening. However, the prepowerstroke state produces little force in this case because negatively strained cross-bridges detach at small strains. We show that the properties of this prepowerstroke state are similar to those of prepowerstroke states proposed by others from different data.

The critical stretch and its velocity dependence are important parameters for defining cross-bridge models. A number of investigators have studied the mechanics and energetics of muscle fibers during stretch, but most of these studies have employed living frog muscle (Hill, 1968; Flitney and Hirst, 1978; Edman et al., 1978, 1981, 1984; Cavagna et al., 1994; Colomo et al., 1988a, 1989b; Lombardi and Piazzesi, 1990; Piazzesi et al., 1992; Månsson

---

1994; Tsuchiya and Sugi, 1988). More recently, skinned mammalian fibers have also been used (Stienen et al., 1992). Measurement of the critical stretch requires sarcomere length control, so that the compliance in the ends of the fiber is not added to the measurement. Critical stretch has been measured with sarcomere length control in living frog fibers (Lombardi and Piazzesi, 1990), but not in mammalian fibers.

We stretched fully activated glycerinated rabbit psoas fibers over a wide range of constant velocities (0.1–3.0 lengths/s), under sarcomere length control, using an apparatus designed to eliminate stray compliance. We measured the critical stretch, the force at critical stretch, stiffness during each phase of the force response, and the velocity dependence of each of these measures. Finally, we measured the response to stretch of fibers in the presence of high levels of vanadate, a phosphate analog that inhibits tension by increasing the fraction of cross-bridges in a prepower-stroke state (Dantzig and Goldman, 1985; Goodno, 1982).

MATERIALS AND METHODS

Fibers

Bundles of psoas fibers $\sim$2 mm in diameter were dissected from New Zealand White rabbits. The bundles were tied to wooden sticks and chemically skinned by incubation at 4°C in 50% glycerol, 0.12 M KCl, 5 mM $MgCl_2$, 5 mM EGTA, and 20 mM 3-(N-morpholino)propanesulfonic acid (MOPS) (pH 7.0). The solution was changed after the first 24 h, and the fibers were stored at -20°C for 2 weeks to 3 months before use. For experimentation, single fibers were dissected from a bundle on a cold glass microscope slide.

Fibers were attached to the apparatus before being lowered into solution. One end of the fiber was laid across an arm (a glass capillary tube) connected to a silicon beam force transducer, and the other end was laid across a metal arm connected to the armature of a motor. The fiber ends that lay on the arms were then fixed with 2.5% glutaraldehyde (Tousimis Research Corporation, Rockville, MD), following the methods of Chase and Kushmerick (1988). Excess glutaraldehyde was removed by vacuum. After fixation, the ends of the fiber were glued to the arms using fingernail polish diluted with acetone. Excess glue was removed by vacuum. The fiber was then lowered into the relaxing bath, and fiber length and thickness were measured with the reticule of a stereo microscope (SMZ-2T; Nikon, Tokyo, Japan). Fiber diameter was estimated by assuming a circular cross section. The length of the unfixed portion of the fiber between the arms varied from 3 to 4 mm, and the fiber diameter ranged from 50 to 100 μm.

Force transducer and motor

The apparatus has been described fully in Pate and Cooke (1988). Briefly, the force transducer (Aksjelskapet Microelectronic, Horten, Norway) with the attached arm had a resonant frequency of $\sim$2.5 kHz when immersed in solution. The motor (model CX-660; General Scanning, Watertown, MA) with attached arm responded to a step position command with an exponential time course, with a time constant of 0.4 ms.

Bathing solutions

Fibers were immersed in a 1-ml well maintained at 10°C, containing a relaxing solution consisting of a rigor buffer (5 mM $MgCl_2$, 1.0 mM EGTA, 20 mM MOPS, pH 7.0), an ATP regenerating system (20 mM

creatine phosphate and 1 mg/ml creatine phosphokinase), 4 mM ATP, and 3 mM inorganic phosphate (P_i). Addition of small amounts of P_i help to stabilize the diffraction pattern, allowing control of sarcomere length by feedback of the pattern. The activating solution also contained 1.1 mM $CaCl_2$. The ionic strength of the relaxing and activating solutions was 112 mM and 115 mM, respectively.

Stock solutions of sodium metavanadate ($NaVO_3$) (EM Science, Gibbs-town, NJ) were prepared at 100 mM, pH 10.0, and boiled immediately before use to minimize polymerization (Goodno, 1982). A small (3% by volume) aliquot of the vanadate stock solution was added directly to the bath containing the activating solution. Changes in the pH of the activating bath were less than 0.1 pH unit as a result of vanadate addition.

Laser diffraction

Initial sarcomere length (L_0) was determined by measuring the distance between the central and first maxima of a diffraction pattern using a 20-mW He-Ne laser (0.632-μm wavelength; Uniphase Corp., Manteca, CA). During the fiber stretch, changes in sarcomere length were tracked by movement of the centroid of the first diffraction maximum across a 15-mm-wide position-sensing photodiode (model SL-15; UDT Sensors, Hawthorne, CA). The photodiode currents were converted to voltages by high-input-impedance operational amplifiers, and the difference was amplified by an instrumentation amplifier with a flat frequency response up to 3 kHz.

Because the intensity of the diffraction pattern varied from fiber to fiber and between trials, the change in photodiode output voltage corresponding to a specified change in position of the diffraction pattern was calibrated immediately before each stretch, whether passive or active. The calibration procedure was as follows. The first maximum of the diffraction pattern was centered on the photodiode by moving the photodiode until the output voltage was zero. The position was also inspected visually, to ensure that the pattern was centered on the photodiode and not offset because of stray light from the central maximum. A baffle was inserted between the bath and the photodiode to block light from the central maximum. The photodiode was then moved by micrometer by 1 or 2 mm from the center, and the voltage from the photodiode was sampled. The calibration varied from 2 to 6 analog-to-digital units/nm of sarcomere length, so that the spatial resolution of the photodiode sarcomere length measurement was 0.2–0.5 nm. If the change in photodiode output with a change in detector position did not exceed an equivalent spatial resolution of 0.5 nm, the fiber was discarded. Diffraction patterns of the discarded fibers were not necessarily more scattered, but instead were weak in intensity. Finally, the photodiode was moved back to center the light pattern (zero voltage) before the fiber was stretched. The fiber was initially calibrated in relaxing solution, activated, and recalibrated in activating solution before stretching.

A major problem in measuring sarcomere length by laser diffraction is that some intensity from the zero-order diffraction maximum may also reach the photodiode, resulting in an erroneous measure of the position of the first diffraction peak. The effect of this contaminating signal was quantified by comparing the strength of the scattered light from the zero-order diffraction pattern to the strength of the first-order diffraction signal. The scatter in the zero-order diffraction pattern was predominantly due to the coverslips that form the walls of the bathing wells and to the bathing solutions through which the laser beam passes, and so was quantified by measuring photodiode output voltages from the laser beam repositioned so that it did not strike the fiber. The scattered light was found to be 2–6% of diffracted light, in both passive and active fibers, so that the error introduced by scattered light does not produce a significant error in the measurement of sarcomere length.

To check that the photodiode measurement accurately reflected sarcomere length, we changed sarcomere length in a relaxed fiber, where end compliance plays a minimal role, and compared the photodiode measurement with that obtained by direct visual observation of the position of the first diffraction maximum projected onto a screen 20 cm from the fiber and with that expected from the imposed fiber length change. In passive fibers, these three measures agreed to within 5%. When this measurement was

made in active fibers, the photodiode measurement agreed with direct observation again to within 5%, but because of end compliance the sarcomere length change was only 35–50% of that expected from the fiber length change. These measurements show that the output of the photodiode provides a reasonable measurement of fiber sarcomere length.

To produce sarcomere length control during a stretch (Fig. 1), the position of the centroid of the first-order diffraction maximum was sampled and converted to sarcomere length. The difference between this estimate of sarcomere length and the command sarcomere length, the error in sarcomere length, was then converted to a fiber length error by multiplying by the fiber length divided by the initial sarcomere length. This fiber length error was used to drive the motor. Departures from linearity in the motor input show corrections made to the length command to achieve ramp

stretches of sarcomeres and indicate the necessity of sarcomere length control. Typically the motor was required to move faster than the average velocity near the beginning of the stretch to compensate for end compliance, as shown in Fig. 1.

The open loop gain was adjusted to drive the feedback system close to the command sarcomere length, while maintaining stability, and was optimized for control at the beginning of the ramp. In addition to the gain we set, the closed loop gain also depended on the compliance in the fiber-machine connections, more compliant connections requiring a larger change in motor position to drive the same change in sarcomere length. The closed loop gain thus varied between fibers, and ranged from 0.35 to 0.75 in the experiments reported here. The dependence of gain on fiber compliance explains the slight curvature we often saw at the long end of our sarcomere length recordings (e.g., *upper trace* in Fig. 2): as the fiber stretched, it became stiffer (less compliant), so that the gain that was adequate to maintain a ramp in sarcomere length at a shorter length became too small to maintain a straight line at longer length. This error, however,
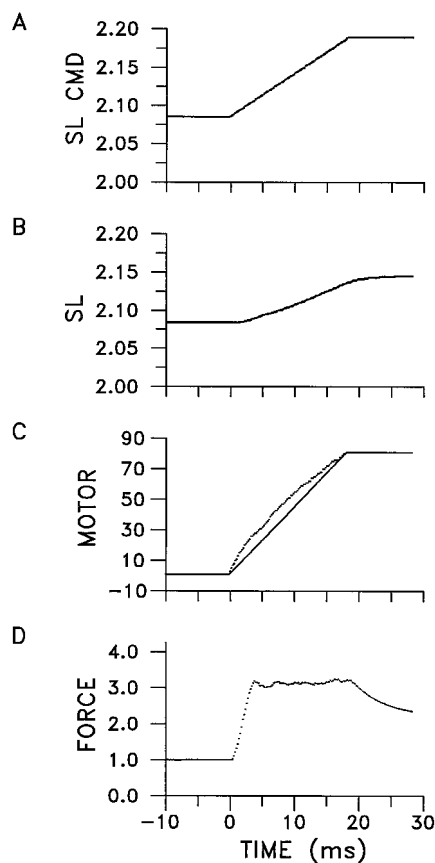

FIGURE 1 Command sarcomere length, measured sarcomere length, motor position, and force for a rapid closed-loop stretch. Sarcomere length is measured from movement of the first-order diffraction maximum on a photodiode and fed back to the computer controlling fiber length. The result is a linear ramp in sarcomere length. In this figure, closed loop sarcomere length control produces a 2.6% stretch at 1.4 L_0/s in response to a 2.0 L_0/s command. The actual stretch velocity is necessarily less than the command velocity as a result of the negative feedback loop. (*Top panel*) sarcomere length (SL) (in mm) requested. (*Second panel*) Actual sarcomere length. (*Third panel*) Motor position (in mm) during the stretch. The straight line is provided for comparison, and the nonlinearity of the motor position demonstrates the necessity for closed-loop control to achieve constant velocity of sarcomere stretch. (*Bottom panel*) The force response (in units of isometric force, P_0) rises in two phases: a large increase in force occurring in the first few nanometers of stretch (here 3.2 P_0 in 6.2 nm/half-sarcomere), followed by nearly constant force for the remainder of the stretch. In some fibers, force continued to rise slowly in this second phase. Data are from a single active rabbit psoas fiber 2.7 mm in length. Sampling rate: 5000 s^{-1}.
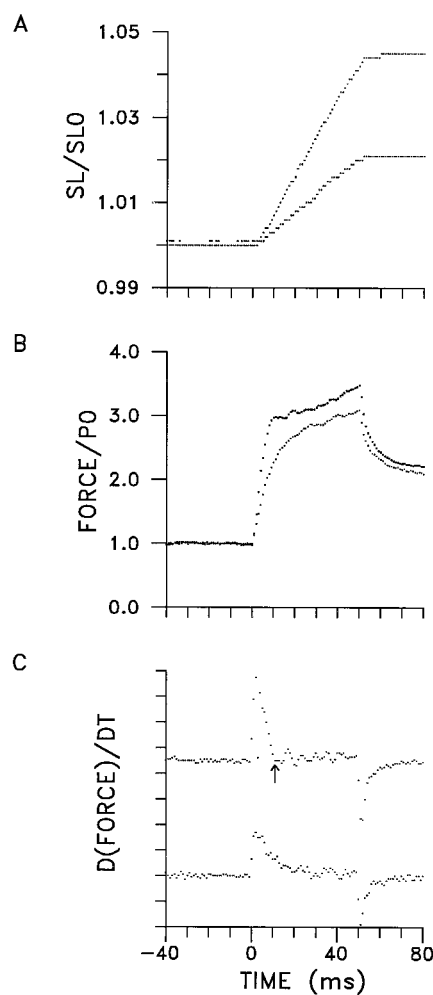

FIGURE 2 Force responses of an active fiber to fast and slow constant velocity stretches. (*Top panel*) Sarcomere length, as measured by laser diffraction, normalized by initial sarcomere length (SL_0). (*Middle panel*) Force, in units of isometric force (P_0). (*Bottom panel*) Rate of change of force, d(force)/dt. In all of the panels, the top trace corresponds to stretch at 0.8 L_0/s, the bottom trace corresponds to stretch at 0.4 L_0/s. Faster stretches produced a clear breakpoint in force, with corresponding zero or zero crossing in the derivative of force (*arrow*). Slower stretches often produced no clear breakpoint. Critical stretch (L_C) and critical force (P_C) are defined as stretch and force at the breakpoint. Sampling rate: 1000 s^{-1}.

does not affect our measurements, as they are made in the first few nanometers of the stretch, during which a constant velocity is well maintained (a straight line fit to the first 90% of the ramp in Fig. 2, for example, fits with $R^2 = 1.0000$). We recorded many trials without sarcomere length control. In these open loop recordings, the rapid rise in force (phase I) and the slower rise (phase II) are still apparent, but the transition is much less distinct: the open loop records looked like the force traces of Stienen et al. (1992).

Data collection

During stretches, fiber force and the position of the first diffraction maximum were sampled at 1 or 5 kHz for 0.6 s by a 486 PC interfaced to the force transducer and photodiode by an analog/digital board (HSDAS-12; Analogic, Wakefield, MA). Input to the motor was calculated by the computer at a rate of 1 kHz based on movement of the diffraction maximum so as to produce the desired change in sarcomere length. For each ramp stretch, the command sarcomere length, actual sarcomere length (photodiode signal), motor input (position), and force were saved during the 50 ms of isometric contraction before stretch, the 3–5% stretch, and the isometric contraction for the remainder of the 600-ms sampling time. The computer program was written in Borland C++ (Version 3.1; Borland International, Scotts Valley, CA).

Experimental protocol

Fibers were mounted and immersed in a relaxing solution. The fiber diameter was measured, and the force reading was set to zero. The fiber was scanned for the clearest diffraction pattern by moving the laser beam across it. If a clean pattern could not be found near the center of the fiber, the fiber was discarded. Initial sarcomere length (L_0) was measured from the diffraction pattern projected on a calibrated screen. L_0 varied from 2.0 to 2.4 μm. The photodiode was then calibrated, and the fiber then stretched at a specified command velocity for 3–5% of L_0 under sarcomere length control, held at the final length for the remainder of the 600-ms sampling time, and returned to the initial length by a slow (0.1 L_0/s) shortening ramp. Stretch velocities ranged from 0.1 to 3.0 L_0/s. The maximum unloaded shortening velocity for glycerinated psoas at 10°C is 1.6 L_0/s (Cooke et al., 1988). Although the measurements of Cooke et al. were made at an ionic strength greater than that used in the present study, maximum shortening velocity has been found to be independent of ionic strength (reviewed in Seow and Ford, 1993). Commanded sarcomere length, actual sarcomere length, force, and voltage input to the motor (corresponding to motor position) were displayed on the computer monitor and used for quality control. If actual sarcomere length was not proportional to command sarcomere length, or if the motor input was anomalous, the data were rejected. In relaxed fibers, the force response was small, typically 2–5% and never exceeding 15% of the force change in activating solution at full stretch (1.05 lengths). If all measurements were in order, the fiber was then transferred to activating solution, and photodiode calibration and ramp stretch of the fiber were repeated. Maximum isometric stress (P_0) was typically 120 kN/m². Once force stabilized at P_0, calibration and stretch were performed as quickly as possible (10–60 s), as the diffraction pattern was not long-lived. For most fibers, only one or two active stretches were possible.

Stretches were also performed on some fibers in the presence of vanadate (V_i). The fractional decrease in isometric force and isometric stiffness produced by 3 mM V_i was determined on five fibers by the following procedure before the stretching experiments. After mounting, each fiber was immersed in a relaxing bath without V_i, and the force reading was set to zero. Fiber stiffness was measured from the change in force resulting from a rapid (<0.5 ms) 0.5% extension of fiber length. The fiber was then transferred to an activating bath without V_i. Once the force had stabilized and been recorded, active fiber stiffness was measured. Then 3 mM V_i was added directly to the activating bath. Force declined over the course of ~60 s, then stabilized. The ratios of the isometric force and

stiffness in the presence of V_i to the isometric force and stiffness without V_i were recorded for each fiber. In the stretching experiments, each fiber was initially immersed in a relaxing bath without V_i. The photodiode was calibrated and the fiber was stretched following the protocol given in the preceding paragraph. The fiber was then transferred to the activating bath containing 3 mM V_i. Force rose initially, then fell. Once the force had stabilized, the photodiode was recalibrated, and the fiber was stretched.

Data analysis

For stretches faster than ~1L_0/s, there was a clear break point in the force record (Fig. 2, *upper traces*). Digital differentiation of force (3-point Lancos differentiating filter; Hamming, 1983) revealed a sharp transition between rates of force rise at this point, with faster stretches often showing a zero crossing in d(force)/dt. The transition time was defined as the time after the beginning of the stretch when the rate of force development (d(force)/dt in Fig. 2) first became zero or negative. Critical strain (L_C) and critical force (P_C) are strain per half-sarcomere and force, relative to P_0, at the transition time. For slower stretches, a transition time was usually much more difficult to define: there was no clear break point, and d(force)/dt revealed no clear transition time (Fig. 2, *lower traces*). We therefore report critical strains only for records in which there was a clearly definable transition. For model parameter identification, it was important to obtained an estimate of P_C at low stretch velocities (<0.5 L_0/s). For these slow stretches, we estimated the break point by fitting tangents to the two phases of force rise (Stienen et al., 1992). However, both the force and d(force)/dt traces in Fig. 2 make it clear that force during phase I is by no means linear, so this method cannot be expected to yield as reliable results.

Stiffness of the isometric fiber was calculated by dividing the increase in force (relative to P_0) after the small length step by the length change per half-sarcomere, as measured from the diffraction record. Because length steps are difficult to distinguish in the diffraction records during a stretch, stiffness during phase II was measured relative to isometric stiffness, by computing the ratio of the force rise in response to the step during Phase II to the force response to the step during isometric steady state (the command step sizes were the same).

The small length steps used to assess fiber stiffness produced transient changes in force. Decay half-times were measured as the time from peak force (at the time of the step stretch) to half the difference between peak force and the force extrapolated from the force trajectory before the steps.

RESULTS

Force response to constant velocity stretch

In activated fibers, the force response to a constant-velocity stretch consisted of two phases: an initial rapid increase occurring over a very small stretch (phase I), followed by a slower rise lasting the remainder of the stretch (phase II). The two phases were much clearer in force responses to stretches faster than ~1L_0/s (Fig. 2, *upper traces*), than in responses to slower stretches (*lower traces*). In the 150–500 ms after the stretch, force declined in two phases well fit by the sum of two exponentials (Colomo et al., 1989a,b; Cavagna, 1993). The faster rate constant was 200 s^{-1}, independent of stretch velocity, and the slower was about an order of magnitude slower.

Critical stretch and force at critical stretch

The break point in the force trajectory, identified in the 39 records with clear-cut zero crossings of d(force)/dt, occurred at a stretch of 7.7 ± 0.1 nm/half-sarcomere (mean ±

SEM). The critical stretch appears to be larger at the slowest velocities of stretch (Fig. 3 *A*), but this difference is not statistically significant ($\alpha < 0.05$).

Force at critical stretch (P_C) increased rapidly with velocity up to $\sim 1 L_0$/s, then leveled off at $3.26 \pm 0.06\ P_0$ ($N = 34$, Fig. 3 *B*). In relaxed fibers, the force response was typically less than 5% and at most 15% of the force change in activating solution, at full stretch (1.05 lengths). The passive component of force at critical stretch (i.e., at 1.008 lengths) was therefore at most 2.4% of the total.

Response to small stretches

Fiber stiffness was evaluated by superimposing small step stretches (command steps of 2.5 nm/half-sarcomere, producing actual steps of 0.7–1.9 nm/half-sarcomere) before, during, and after the constant-velocity ramp and measuring the corresponding increase in force. Steps were imposed 35 ms before the start of the stretch, at 40% and 80% of the stretch, and 10 and 60 ms after the stretch (Fig. 4).

Isometric stiffness (k_0), defined as the ratio of normalized force change to imposed length change, was 0.208 ± 0.014 nm^{-1} ($N = 127$), comparable to the value (0.239 nm^{-1}) measured by Lombardi and Piazzesi (1990) in living frog fibers, using a similar length-step protocol. Stiffness in phase II exceeded isometric stiffness by $15 \pm 3.5\%$ ($N = 102$), similar to the 10–20% increase found by Lombardi
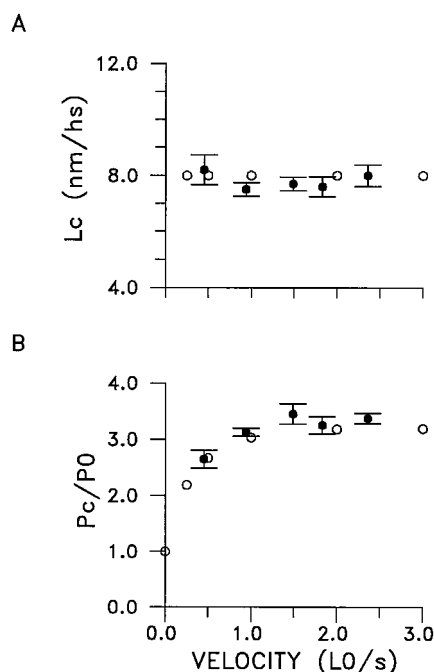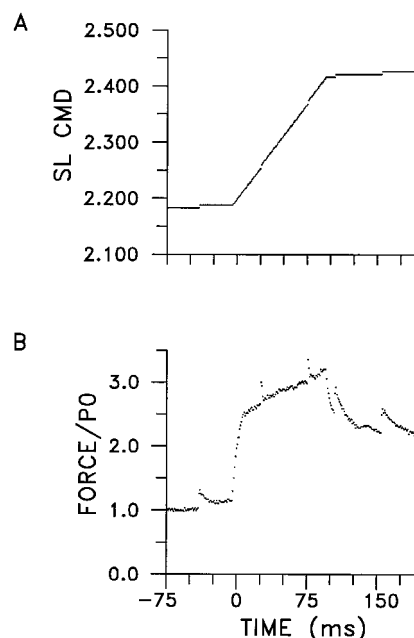
FIGURE 4　Force response to small length steps imposed before, during, and after the stretch. (*Top panel*) Command sarcomere length, used in a feedback loop to determine the input to the motor controlling fiber length. Small steps are commands for 2.5 nm/hs, eliciting actual steps of ~ 1.0 nm/hs (closed loop gain was 0.41). (*Bottom panel*) Force response in units of isometric force (P_0). The small steps in length produce simultaneous increases in force, which were used to calculate fiber stiffness. Note the rapid return to the previous force trajectory during stretch, in contrast with the slow kinetics before and after stretch. Initial fiber length: 3.57 mm; initial sarcomere length: 2.182 μm; stretch velocity: 0.4 L_0/s; sampling rate: 1000 s^{-1}.

and Piazzesi (1990). It should be noted that the speed of our motor (2.5 kHz) and slow sampling rates (1 or 5 kHz) may not be adequate to measure stiffness accurately, especially during phase II. If the force response to a step is falling with a time constant of 1.5 ms (as during phase II in Table 1), sampling at 5 kHz may miss the early response, amounting to 20% of the force, thus underestimating stiffness by 20%. Stiffness returned to isometric stiffness within 10 ms after the stretch ($1.04 \pm 0.03\ k_0$, $N = 128$) and remained the same ($1.081 \pm 0.04\ k_0$, $N = 107$) 50 ms later.

The rate of decay during phase II of the stretch was much faster than during the isometric steady state, or during the decline in force after the stretch (Table 1 and Fig. 4). The decay rate was the same throughout phase II (assessed at 40% and 80% of stretch) and was fast in passive fibers.

FIGURE 3　Dependence of critical stretch (*A*) and force at critical stretch (*B*) on stretch velocity. (*A*) Critical stretch, L_C, in nm/half-sarcomere, plotted as a function of the velocity of stretch, in L_0/s. (*B*) The force measured at critical stretch, P_C, relative to isometric force, P_0. In both figures, open circles represent model predictions, and filled circles represent mean data values ($\pm$ SEM), grouped in the velocity bins listed in Table 1.

TABLE 1　Half-time of force decay after step stretches (mean ± SEM)

Time of length step	Half-time of force decay after step (ms)
Before stretch	3.0 ± 0.1 ($N = 127$)
40% of stretch (phase II)	1.4 ± 0.1 ($N = 102$)
80% of stretch (phase II)	1.6 ± 0.1 ($N = 127$)
10 ms after stretch	4.5 ± 0.2 ($N = 127$)
60 ms after stretch	7.8 ± 0.4 ($N = 125$)

Effect of vanadate

To assess the contribution of prepowerstroke states to force rise in phase I, we stretched fibers in an activating solution containing 3 mM vanadate. Vanadate (V_i), an analog to phosphate, forms a stable complex with myosin and ADP, thus increasing the fraction of cross-bridges in a prepowerstroke state (Goodno, 1982; Dantzig and Goldman, 1985; Chase et al., 1993). The reduction in isometric force and stiffness after the addition of V_i was monitored in five fibers before the stretch experiments. The addition of 3 mM V_i lowered isometeric force to 7.6 ± 0.5% of control P_0 and lowered isometric stiffness to 10.4 ± 0.6% that of control stiffness.

Fibers stretched in activating solution plus 3 mM V_i demonstrated both phases of force rise (Fig. 5). V_i (3 mM) attenuated P_C much less than isometric force. At stretch velocities exceeding $1.0L_0$/s, P_C was 0.82 ± 0.06 times control P_0 ($N = 12$), as compared to 3.26 ± 0.06 P_0 ($N = 34$) in fully active fibers. Thus, in 3 mM V_i the ratio of P_C to isometric tension was ~10, compared to 3.2 in control fibers. As discussed below, we interpret this result as evidence that the prepowerstroke state contributes substantially to the increase in force observed when muscles are stretched.

DISCUSSION

Comparison with previous data

Critical stretch

An important experimental parameter for constraining models of cross-bridge mechanics is the distance the sarcomere has been stretched when the phase transition occurs. An accurate determination of this distance requires sarcomere control to eliminate the fiber compliance that is external to the sarcomere. Such experiments have been performed with living frog muscle by Lombardi and Piazzesi (1990), who stretched tibialis anterior fibers at constant velocities and found that force overshot its steady-state value at the transition between phase I and phase II. They measured the stretch at peak of force overshoot (l_p). Their Fig. 4 shows that l_p declines as stretch velocity increases and asymptotes between 9 and 12 nm/half-sarcomere (above 0.56 μm/s per half-sarcomere). Our studies are the first to apply sarcomere length control to mammalian fibers during stretch. Our value for L_C (8 nm) is only a little shorter than the value of l_p for living frog fibers (9–12 nm). Almost all of our data are at velocities (>$1L_0$/s) at the upper end of the velocity range they tested. In the absence of sarcomere length control, the critical stretches were longer (14–16 nm/half-sarcomere) for frog fibers (Edman et al., 1981, 1984; Colomo et al., 1988, 1989) and for permeabilized rabbit psoas fibers, probably because of the contribution of compliances in series with the fiber (Stienen et al., 1992). In fact, if we had stretched without sarcomere length control, we would have obtained a value for L_C similar to that of Stienen et al. (1992), because in our experiments the motor moved ap-
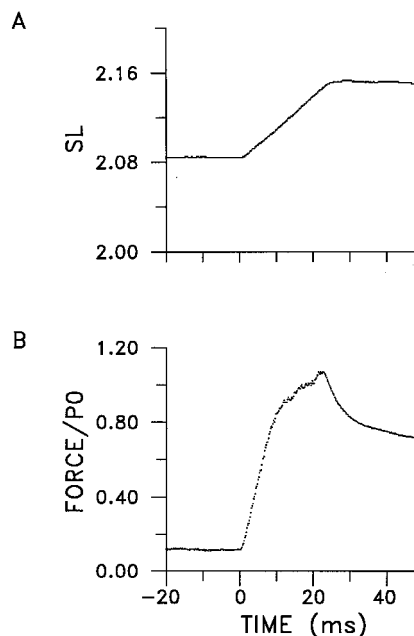

FIGURE 5 Force response of a single fiber activated in 3 mM vanadate. (*Top panel*) Sarcomere length (μm) during a stretch of 3% L_0 at 1.4 L_0/s. (*Bottom panel*) Force response. In this fiber, the isometric force in vanadate was only 12% of the isometric force in activating solution without vanadate (P_0), but the force rise in phase I (P_C) was still large (0.82 P_0, or seven times the isometric force in vanadate). Initial fiber length: 2.91 mm; sampling rate: 5000 s^{-1}.

proximately twice as far as did the sarcomere length. We conclude that the critical stretch in mammalian fibers is similar to that in frog fibers, and that it is independent of velocity from $1L_0$/s to at least $3L_0$/s.

Force at critical stretch

Generally, investigators find that the steady-state force at high lengthening velocity in living frog fibers is ~$2P_0$, independent of velocity above 0.5–1 μm/s per half-sarcomere (Sugi, 1972; Flitney and Hirst, 1978; Edman et al., 1978, 1981, 1984; Cavagna, 1993; Cavagna et al., 1994; Colomo et al., 1988a,b, 1989a,b; Lombardi and Piazzesi, 1990; Piazzesi et al., 1992; Månsson 1994; Tsuchiya and Sugi, 1988). At lower velocities, steady-state force is a rapidly increasing function of velocity, with half-saturation at ~0.5 μm/s per half-sarcomere.

In permeabilized rabbit psoas at 15°C, Stienen et al. (1992) found maximum forces asymptoting at ~$2P_0$ for isovelocity stretches up to $1L_0$/s. We found a value half again as large. However, much of the difference is probably due to three factors: temperature, phosphate, and ionic strength. Cavagna (1993) found a strong temperature dependence of the force rise during stretches of living frog fibers. Force rose to $2P_0$ at 4°C and to only 1.4P_0 at 14°C. This change was due to a strong temperature dependence of P_0 and little temperature dependence of the absolute force produced by stretch. Similar results were found by Edman et

al. (1984). In preliminary experiments, we find a similar temperature dependence in skinned rabbit psoas fibers.

Our relatively large P_C may also be partially due to the higher phosphate concentration at which we worked (3 mM added P_i in our experiments, 0 mM in Stienen et al.). Added P_i reduces P_0 to a greater extent than stretch force (Stienen et al., 1992; Iwamoto, 1995). Stienen et al. added 15 mM P_i and found an attenuation of isometric force to 58% of control and an attenuation of stretch force to 71% of control. Interpolating from Stienen's data and using the logarithmic relationship between P_i and P_0 determined by Pate and Cooke (1989), we estimate that the added 3 mM P_i in our experiments may have increased the relative force enhancement during stretch by ~10%, by lowering P_0 more than P_C.

The ionic strength of our activating solution, 115 mM, is reasonably similar to physiological ionic strength (140–180 mM; Gordon et al., 1973; Godt and Maughan, 1988), but lower than the 200 mM ionic strength used by Stienen et al. (1992) in the previous study of skinned mammalian fibers. Ionic strength varies the relative populations of pre- and postpowerstroke states. In relaxed fibers, low ionic strength increases the population of a weakly bound attached state (Brenner et al., 1982; Schoenberg, 1991). In activated fibers, a prepowerstroke state is populated by high ionic strength. These two prepowerstroke states are probably not equivalent (Seow and Ford, 1993; Iwamoto, 1995). Experiments on active fibers have shown that fiber stiffness is less affected by ionic strength than is isometric force (Piazzesi et al., 1994; Seow and Ford, 1993; Månsson, 1989), suggesting that it is not the number of attached cross-bridges that is altered by ionic strength, but the distribution between pre- and postpowerstroke states. The moderately low ionic strength of our bathing solutions would therefore be expected to raise isometric force, with little effect on stretch force (Piazzesi et al., 1994; Månsson 1994) or maximum shortening velocity (reviewed in Seow and Ford, 1993). We performed control stretch measurements on fibers bathed in a solution with ionic strength raised to 200 mM by the addition of 85 mM KAc, for comparison with the data of Stienen et al. (1992). Increased ionic strength lowered the isometric force by 30% but had no effect on force during stretch.

Phase II force rise

A continued force rise after the critical stretch was sometimes but not always present in our data. Force tended to continue to rise during slow but not necessarily during fast stretches. Stienen et al. (1992), also using permeabilized rabbit psoas fibers, consistently measured monotonic force rise. However, stretches of permeabilized rabbit soleus fibers (Stienen et al., 1992) and living frog fibers (Lombardi and Piazzesi, 1990) display an overshoot in force, followed by steady force. Edman et al. (1978, 1996) also using living frog fibers, sometimes recorded force rise after the break point, and other times did not. We conclude that the phase

II force rise depends on the preparation, and that it may be due to factors outside the cross-bridge, such as sarcomere heterogeneity, as proposed by Morgan (1990) and by Edman and Tsuchiya (1996). This portion of the data is not considered in the model proposed below, which would predict a constant force in phase II, due to cross-bridge kinetics alone.

Step responses

Piazzesi et al. (1992) imposed steps of different sizes, both lengthening and shortening, on stretched living frog fibers. During slow stretches they recorded four phases of force recovery, similar to those of Huxley and Simmons (1971). For faster stretches the force response was dominated by phase IV, reflecting rapid attachment and detachment. For stretches at speeds comparable to those we imposed (faster than 1 μm/s per half-sarcomere), the rate of recovery was comparable to what we measured (0.4–0.7 ms for 63% recovery; their figure 23).

Recovery of force and stiffness after stretch

Like Cavagna (1993), we found that the force decline in the first few hundred milliseconds after stretch was well fit by two exponentials. The fast, early component had a rate constant of ~200 s^{-1}, and the second was at least an order of magnitude slower.

Although others have measured stiffness during stretch with much greater time resolution than ours (Piazzesi et al., 1992), we know of no data comparable to ours investigating the recovery of stiffness after a stretch. Both the magnitude of the force response to a step change in length and the rate of decay of that response recover within tens of milliseconds of the end of the stretch.

Effect of vanadate

In addition to creating a long-lived prepowerstroke state (Goodno, 1982; Dantzig and Goldman, 1985; Chase et al., 1993), vanadate (V_i) also appears to reduce the total number of attached cross-bridges: both isometric force and stiffness are decreased in the presence of V_i, although at low temperatures (10°C), the reduction of stiffness is somewhat less than the reduction of force (this paper; Chase et al., 1993). Thus stretch force is reduced by V_i, presumably because of the decrease in number of attached cross-bridges, but much less than is isometric force, because V_i holds cross-bridges in a prepowerstroke state that exerts low isometric force but high force during stretch.

Model

Data to be fit

Any model of fiber mechanics during isovelocity stretch must account for the following data.

1. Force rises rapidly in the first few nanometers per half-sarcomere of stretch. Force may continue to rise after this initial phase but does so relatively slowly, if at all. The transition in force rise occurs after a critical amount of stretch that is independent of stretch velocity.

2. Fibers exhibit mechanical rectification. Both force and stiffness decline with increasing velocity during shortening, but the response to stretch is production of large forces (up to $2-3P_0$), with only a moderate change (10–20% increase) in stiffness.

3. The kinetics of the force response to small length steps are much faster during the stretch than before or (>10 ms) after the stretch.

4. Addition of P_i or P_i analogs reduces isometric force to a greater extent than the force generated during stretch.

5. After the stretch, in a fiber held isometric, tension relaxes with a fast phase at a rate of ~ 200 s^{-1}, followed by a slower decline to P_0. There is rapid (<10 ms) return of stiffness to its prestretch value.

Previous models

The simplest cross-bridge model, proposed by A. F. Huxley in 1957, does not accurately describe force during stretch, because it predicts a decrease in steady-state force with increasing stretch velocities. By modifying the off rate, Zahalak (1981) was able to fit a Huxley two-state model to steady-state lengthening data. However, to maintain a large force at high stretch velocities, it was necessary to allow some cross-bridges to extend to extreme lengths, exceeding the assumed repeat distance between actin sites. Harry et al. (1990) attempted several variations on the 1957 Huxley model to fit their data on steady-state force as a function of stretch velocity. They found that the introduction of a maximum allowable cross-bridge strain implied that force would decrease as stretch velocity increased. Otherwise, rapid attachment during stretch would be required to maintain force at high velocities. Such rapid attachment is, however, inconsistent with shortening of the Huxley 1957 model.

The necessity of a region of rapid attachment for maintenance of steady force during stretch has long been recognized (Hill, 1968; Flitney and Hirst, 1978; Güth and Kuhn, 1978; Griffiths et al., 1980). Colomo et al. (1989b) also noted that the detachment rate must be small over some range of cross-bridge strain to keep that range populated at high velocities of stretch. However, rapid attachment will also maintain high fiber stiffness and force during shortening.

The major problem in developing a model that incorporates these concepts is that the rapid attachment into a force-generating state, required to maintain force during rapid stretches, also maintains force and stiffness during rapid shortening. Lombardi, Piazzesi, and colleagues (1990, 1992, 1995) developed models that solved this problem by proposing a new detached state that is populated only by a rapid detachment of highly strained cross-bridges during

stretch. The rapid reattachment of cross-bridges from this state maintains a high force during stretch. Because this state is not populated during shortening, force and stiffness decrease with increasing shortening velocity. Thus this model is consistent with both lengthening and shortening mechanics. Månsson (1994) put forward a similar model, also with a special detached state entered only during stretch. Based on the observation that stretch force is unaffected by high extracellular tonicity while isometric force is depressed, Månsson further proposed that stretch force is produced by the "low force" state that precedes a high force state during isometric cycling.

Proposed model

We propose a new model to account for the mechanics of muscle during steady stretch. The model is, in essence, a synthesis of the biochemically detailed model of Pate and Cooke (1989), with some of the kinetic concepts proposed by Lombardi, Piazzesi, and colleagues (1990, 1992, 1995) and by Månsson (1994). Our new model involves only biochemically identified states and hypothesizes no special detached state. Based on the observation that force rise during stretch is less affected by P_i and V_i than is the isometric force, we propose that the force during rapid stretch is produced primarily by cross-bridges in a prepowerstroke (AMDP) state. We choose rate constants associated with this state such that the cross-bridges in it act as mechanical rectifiers, producing large forces during stretch and small forces during shortening. In addition, the model reconciles the critical length with recent measurements of the powerstroke length and with structural models of myosin function (Molloy et al., 1995; Rayment et al., 1993).

The Pate and Cooke model has three attached states. During shortening or under isometric conditions, cross-bridges first attach in a prepowerstroke state (AMDP), at the beginning of a region of positive force production. P_i release results in transition to a strongly bound state (AMD). ADP release and detachment due to ATP binding to the AM state occur at the end of the region of positive force production. The known energetics of the actin-myosin-nucleotide interaction in solution define the free energy minima of states in the fiber (as in the model of Eisenberg et al., 1980). Pate and Cooke assumed that attached cross-bridges act as Hookean springs. The free energy minima and an assumed elastic force constant of $0.56RT$ nm^{-2} then determine the free energy profiles of the model. Pate and Cooke chose transition rate functions (Table 3) to fit isometric and shortening data. The critical kinetic assumptions that make shortening mechanics work in this model are MDP cross-bridges bind very rapidly to actin over a short range, around the minimum free energy of the AMDP state; the transition from weakly to strongly bound states is limited by the release of phosphate, at ~ 50 s^{-1}; transition from the AMD state to AM is very slow until near the end of the power stroke, then is quite fast; detachment from AM to MT is quite rapid over the entire power stroke, and very rapid for $x < 0$. Our model

retains these kinetic assumptions, but with simple piecewise constant transition rates (Table 3), as it is intended to demonstrate feasibility, rather than to fit data precisely. The detached states MDP and MD are lumped into the model, so an attachment rate from MD to AMD ($R_{24} = 60$ s^{-1}) is included. During stretch, cross-bridges are assumed to detach from the AMD state to MD with the reverse rate constant (R_{42}). The Pate and Cooke model does not include an off rate from AMD to MD, because this detachment is not important in shortening.

The essential changes in rate constants required to implement our new lengthening mechanism are in the assumed transitions between the prepowerstroke state (AMDP) and its detached state (MDP). During steady-state lengthening, AMDP cross-bridges are assumed to detach at or before a maximum strain, implemented by a very large detachment rate constant for distortions beyond 8 nm. Once detached, MDP cross-bridges are assumed to reattach rapidly with a rate constant (R_{23}) that is large in a region of little strain (2.26 nm $\leq x \leq 4.0$ nm). Rapid detachment and reattachment has been shown to occur for both strongly and weakly bound cross-bridges (Brenner et al., 1986). A relatively slow detachment rate in a region of positive force production (4 nm $\leq x \leq 8$ nm) allows the AMDP bridges to produce large forces during stretch. With these changes, the AMDP state becomes a mechanical rectifier. The rapid attachment rate populates the positive force production region of the AMDP state during lengthening, permitting forces up to $3P_0$. The very rapid detachment at $x > 8$ nm ensures that force reaches a plateau as lengthening velocity increases. Rapid attachment also occurs during shortening or isometric contraction, but the AMDP state produces little force under these conditions because positive- and negative-force-producing regions are about equally populated, because cross-bridges are assumed to detach rapidly from small negative strains.

To account for the short critical length we measured, and to keep total cross-bridge distortion consistent with current structural models of the contractile proteins, we compressed the x scale (cross-bridge distortion), so that the free energy minimum of the AMDP state was at 4 nm, instead of the 7.5 nm assumed by Pate and Cooke. This modification does not affect shortening behavior, because "the model is invariant with respect to linear transformation of all values of distortion," as Pate and Cooke point out. Maintenance of the same free energy scale, but a compressed x scale, requires a larger elastic force constant, $1.8kT$ nm^{-2} per cross-bridge.

The model has a power stroke of 4 nm. The ultimate strain of the prepowerstroke (AMDP) state is also assumed to be 4 nm (beyond its zero-force length of 4 nm), so that cross-bridges are assumed to be distorted over a range of at most 8 nm, from isometric to rapid stretch. These distances are compatible with current structural models of the contractile apparatus, which suggest that force is produced by the rotation of the 8-nm neck region of myosin (Rayment et al., 1993), and consistent with in vitro motility assays (Molloy et al., 1995).

Simulations

The model with free energy functions as shown in Fig. 6 and listed in Table 2, and with transition rate constants given in
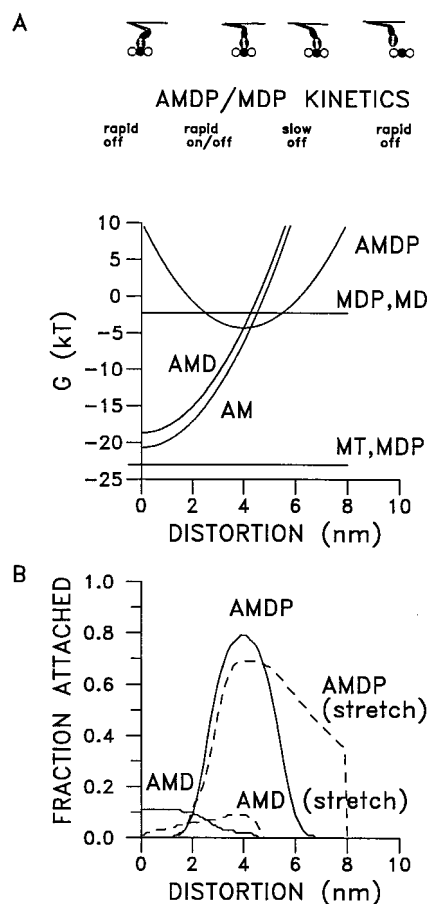

FIGURE 6 Kinetic mechanism and distributions of attached cross-bridge states for lengthening and isometric contraction. Free energy functions for the AM, AMD, and AMDP attached states and a lumped (MD, MDP, MT) detached state are shown as a function of cross-bridge distortion at the top of the figure. Abbreviations: A, actin; M, myosin; D, ADP; T, ATP. Free energy functions are the same as those in Pate and Cooke (1989), with the exception that the distortion axis is compressed so that the model is compatible with an observed critical length (L_C) of 8 nm. Large forces during lengthening are primarily explained by the kinetics of the AMDP/MDP transitions, which are outlined at the top of the figure. The populations of AMDP and AMD, the two states that generate force during stretch, are shown in the bottom figure under isometric conditions (——) and during steady-state lengthening at 1 L_0/s (– – –). The AM state is not significantly populated during stretch, and so is omitted for clarity. During isometric contraction or shortening, cross-bridges in the AMD state produce most of the force, as those in the AMDP state are distributed nearly equally over negative and positive force-producing strains, and they have a rapid off rate at $x < 2.26$ nm. During lengthening, the population of the AMD state declines, and the population of the AMDP state shifts to positive force-producing distortions, with most of the force produced by AMDP states between 4 and 8 nm, which remain attached because of a relatively slow off rate. A steady-state population in AMDP states is maintained by rapid detachment at $x > 8$ nm and rapid reattachment of these detached cross-bridges for 2 nm $< x < 4$ nm. Distances in this figure pertain to cross-bridges only and do not account for actin compliances. States, free energy functions, and rate constants used in the simulations are listed in Tables 2 and 3.

TABLE 2 Free energies as functions of distortion

$G_1(x) = 0kT$
$G_2(x) = -2.3kT$
$G_3(x) = (\kappa/2)(x - 4)^2 - 4.3kT$
$G_4(x) = (\kappa/2)x^2 - 18.7kT$
$G_5(x) = G_3(x) - 2.0kT$

Subscripts correspond to states as follows: 1, MT; 2, MDP, MD; 3, AMDP; 4, AMD; 5, AM. $\kappa = 1.8\ kT/nm^2$. ΔG_{ATP} is assumed to be $-23kT$.

Table 3, was simulated in Borland C++ on a 486 PC, using the method of characteristics (Carrier and Pearson, 1976). Fig. 3 *B* illustrates that the model fits steady-state force as a function of velocity.

Simulation of a force transient during stretch at $1.5L_0/s$ (compared with data in Fig. 7 *A*) shows the transition from the early, rapid phase of force rise to a steady state. The phase transition in force occurs when the AMDP cross-bridges fill their steady-state distribution for stretch, i.e., when the right end of the distribution is stretched from 4 nm to 8 nm. The critical length L_C is thus a measure of the maximum stretch of cross-bridges in the AMDP state. L_C in the simulation is 8 nm, with 4 nm due to stretch of cross-bridges, and the remaining 4 nm due to stretch of the compliant actin filament (Goldman and Huxley, 1994). Thus a stretch of 4 nm per cross-bridge corresponds to a stretch of 8 nm/half-sarcomere. In the following discussion all distances described in the model are for the cross-bridges only, and a comparison with data must take actin compli-

ance into account. After the transition, cross-bridges broken off at the ultimate length quickly reattach, with highest probability at low strain (near $x = 4$), and the rapid on rate into the AMDP state at low strain ensures a steady state. The AMD population also undergoes a transition. AMD cross-bridges break off once their free energy exceeds that of the detached MD state. At high speeds of stretch ($>1L_0/s$), reattachment from MD to AMD is not fast enough to repopulate the AMD state fully, so force from AMD declines as the isometric distribution breaks off and is not replaced.

Relaxation from the steady-state cross-bridge distributions after the stretch also has two parts. The AMDP cross-bridges return to the isometric, zero-force distribution with a rate constant of 200 s^{-1}, chosen to match the fast component of force decline at the end of the stretch. Cross-bridges without P$_i$ also reattach, to reestablish isometric force. The slow decline of force at the end of stretch is thus not simulated by this model.

The mechanical rectification property of the AMDP state, simulated by itself, is exhibited in Fig. 7 *B*. During lengthening, the rapid on rate at negative distortions of this state populates it, and the slow off rate from 4 to 8 nm keeps it populated, producing large force. During shortening, the rapid off rate for sizable negative distortions ensures that cross-bridges in this state produce little force.

The slow component of force decline after stretch is not explained by our model, nor is the long-lasting force en-

TABLE 3 Rate constants (s^{-1}) as functions of distortion (nm)

This model		Pate and Cooke (1989)	
$R_{32}(x) = 10^4$ s^{-1}	$x \geq 8.0$	$= R_{23}\exp(G_3 - G_2)/kT$[§]	
$= 200$	$4.0 \leq x < 8.0$		
$= 1.35 \times 10^3$	$2.26 \leq x < 4.0$		
$= 10^4$	$x < 2.3$		
$R_{23}(x) = R_{32}\exp(G_2 - G_3)/kT$[§]		$= 5 + 500 \exp[-0.8(x - 7.5)^2]$	$x > 0.0$
		$= 0$	$x < 0.0$
$R_{34}(x) = 50$ s^{-1}	$x \leq 4.0$	$= 50$ s^{-1}	$x \geq 7.5$
$= 0$	$x > 4.0$	$= 2000 - 260x$	$x < 7.5$
$R_{45}(x) = 250$ s^{-1}	$x \geq 0.0$	$= 2$ s^{-1}	$x \geq 3.7$
$= 10^3$	$x < 0.0$	$= 273.3 - 73.3x$	$1 \leq x < 3.7$
		$= 750 - 550x$	$0 \leq x < 1$
		$= 750$	$x < 0$
$R_{51}(x) = 10^3$ s^{-1}	$x \geq 0.0$	$= 10^3$ s^{-1}	$x \geq 0$
$= 10^4$	$x < 0.0$	$= 10^3 - (1.4 \times 10^5)x$	$-0.1 \leq x < 0$
		$= 1.5 \times 10^4$	$x < -0.1$
$R_{12}(x)$*		$= 100$ s^{-1}	
$R_{24}(x) = 60$ s^{-1}	$x \geq 0.0$	[#]	
$= 0$	$x < 0.0$		

Subscripts correspond to states as follows: 1, MT; 2, MDP; 3, AMDP; 4, AMD; 5, AM. Reverse rates are from $a_{ji} = a_{ij}\exp(G_j - G_i)/kT$, where the free energies are as listed in Table 2.
*Not applicable in this model, as states 1 and 2 are lumped.
[#]Not applicable in Pate and Cooke, as there is no MD state.
[§]The current model specifies R_{32}, whereas the Pate and Cooke model (1989) specifies the reverse rate R_{23}.
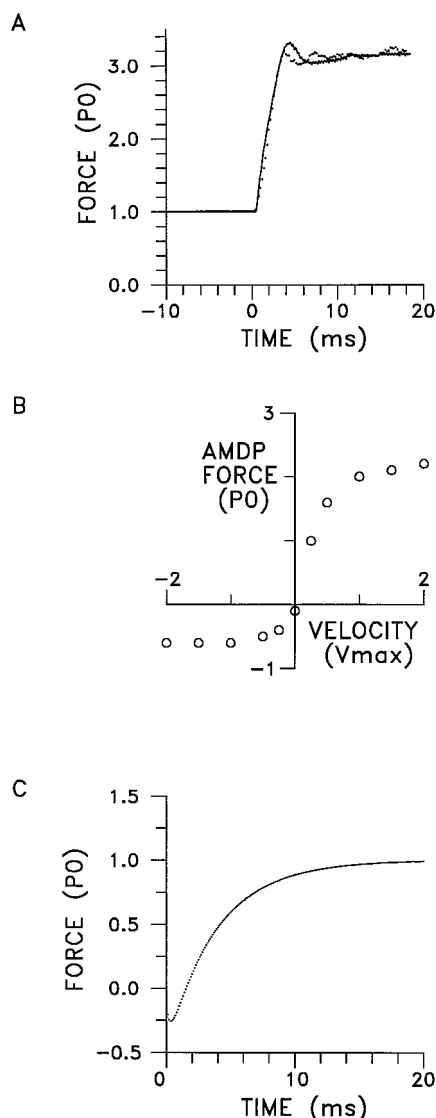
FIGURE 7   Model simulations. (*A*) Force as a function of time during and after a $1.5L_0$/s stretch, simulated using the full model with free energy functions and rate constants as listed in Tables 2 and 3 (*solid line*), overlaid on force data from a psoas fiber. The response to ramp stretch is in two phases: a fast rise from P_0 to over $3P_0$, occurring over the first 8 nm/half-sarcomere of stretch, followed by steady force production. The slight overshoot in force is due to a small difference in the rate of rise in force from prepowerstroke (AMDP) cross-bridges and the rate of fall in force from AMD cross-bridges. In the simulation, a compliance due to actin filaments equal to the cross-bridge compliance is assumed, so that the critical stretch is the sum of 4-nm cross-bridge motion plus 4-nm actin compliance. The apparent noise in the simulation is numerical fluctuation, due to the integration method. (*B*) The prepowerstroke (AMDP) state, simulated alone, produces large positive forces during lengthening, but small negative forces during shortening. This mechanical rectification is due to the slow detachment of AMDP cross-bridges as they are strained positively (between 4 and 8 nm distortion), compared to the fast detachment of AMDP cross-bridges strained negatively (between 4 and 2 nm distortion; see Fig. 6). Force from prepowerstroke cross-bridges during steady-state lengthening asymptotes at high stretch velocity because no cross-bridge can extend beyond a maximum strain (8 nm).

hancement by stretch, nor the force rise sometimes observed in phase II. All of these may occur because of mechanisms beyond the level of a single cross-bridge or even a single sarcomere, and all have been attributed to inhomogeneities between lengths of sarcomeres in series (Morgan, 1994; Edman and Tsuchiya, 1996).

While our model explains the stretch-induced increase in force by postulating different kinetics of the prepowerstroke state when stretched, our data do not exclude the possibility that stretch alters the actomyosin interaction by changing the thin filament.

Data explained by this model

1. The observed effects of added phosphate or phosphate analogs motivated important aspects of the model, and the model simulates these effects well. Phosphate (Iwamoto, 1995; Stienen et al., 1992; Elzinga et al., 1989) and analogs (this paper) affect P_C much less, because the AMDP state they populate produces most of the force during rapid stretch. A simulation of the model with sufficient P_i to drop isometric tension to 50% of control showed that P_C was lowered modestly to two times control P_0.

2. The 10–20% increase in fiber stiffness (Lombardi and Piazzesi, 1990) during rapid stretch is explained in the model by an increase in cross-bridge number during stretch, as more cross-bridges are added to the AMDP state. A 20% increase in fiber stiffness is accomplished by a 50% increase in the number of attached cross-bridges, assuming that half the fiber compliance is in actin, as described above.

3. The model explains the changing kinetics of force responses to the stiffness-testing steps (Table 1). Under isometric conditions, the force response is dominated by the slow kinetics of the AMD state. Stretch populates a prepowerstroke AMDP state, which has very rapid attachment and detachment rates. The very rapid decay in force during steady-state rapid stretch occurs because even a small step moves some of the AMDP cross-bridges past their ultimate length ($x = 8$ nm). These cross-bridges also reattach rapidly, so that force does not drop below the steady-state level. During slow stretch, the kinetics of force responses to stretch may be intermediate between those for fast stretch and isometric (cf. Piazzesi et al., 1992).

4. The rapid return to initial conditions after stretch, including return to isometric stiffness, and to a slower rate of force decline after a step in length, are accounted for by the 200 s^{-1} detachment rate for the strained AMDP cross-bridges (cf. Colomo et al., 1989b). The rate of detachment from the high-force state also determines the velocity required to populate this region. At very slow stretches cross-bridges carried into this region are detached, whereas at very high velocities they are carried through the region and detached beyond the ultimate strain. The velocity of half-saturation occurs at $\sim 0.5L_0$/s, or at a relative filament velocity of 600 nm/s. A simple calculation shows that half-saturation occurs at a velocity approximately equal to the rate constant of detachment times the length of the

region in question. This would suggest a region ~3 nm long, close to the length of the region suggested by the critical length. Thus a rate constant, chosen to fit force decline after stretch, also explains how the increase in force depends on velocity.

5. Piazzesi et al. (1992) found that a rapid step shortening by 2 nm is sufficient to bring force to zero. The distribution of cross-bridges in the force-producing state during isometric contraction (AMD) is consistent with this measurement: they are assumed to be equally distributed over 4 nm, so that step shortening of the cross-bridges by 2 nm (shortening of the fiber by 4 nm per half-sarcomere, assuming half the compliance of the fiber is in actin) would bring their force to zero. A step of 2 nm would carry the distribution of prepowerstroke (AMDP) cross-bridges, distributed between 2 and 6 nm during isometric contraction (Fig. 6), into a region of very rapid detachment (0–4 nm), so that they would not contribute force.

6. The model accounts for the low rate of hydrolysis of ATP in stretched fibers (Abbott and Aubert, 1951), because force during stretch is generated by a state that precedes P_i release (the AMDP state).

7. Finally, the model predicts a small negative force production early in activation, as the negative force-producing region of the prepowerstroke state has by far the fastest on rate. This may account for the observation of latency relaxation, the reduction of force observed in muscle after stimulation and just before a twitch (Abbott and Ritchie, 1951).

Thus a simple model based on known biochemical states and structural features can account for a variety of observations of the mechanics of active fibers, including the magnitude, time, and velocity dependence of force and stiffness during both stretch and shortening.

REFERENCES

Abbott, B. C., and X. M. Aubert. 1951. Changes in energy of a muscle during very slow stretch. *Proc. R. Soc. Lond. Biol.* 139:104–107.

Abbott, B. C., and J. M. Ritchie. 1951. Early tension relaxation during a muscle twitch. *J. Physiol. (Lond.).* 113:330–335.

Brenner, B., J. M. Chalovich, L. E. Greene, E. Eisenberg, and M. Schoenberg. 1986. Stiffness of skinned rabbit psoas fibers in MgATP and MgPP$_i$ solution. *Biophys. J.* 50:685–691.

Brenner, B., M. Schoenberg, J. M. Chalovich, L. E. Greene, and E. Eisenberg. 1982. Evidence for cross-bridge attachment in relaxed muscle at low ionic strength. *Proc. Natl. Acad. Sci. USA.* 79:7288–7291.

Carrier, G. F., and C. E. Pearson. 1976. Partial Differential Equations: Theory and Technique. Academic Press, New York.

Cavagna, G. A. 1993. Effect of temperature and velocity of stretching on stress relaxation of contracting frog muscle fibres. *J. Physiol. (Lond.).* 462:161–173.

Cavagna, G. A., N. C. Heglund, J. D. Harry, and M. Mantovani. 1994. Storage and release of mechanical energy by contracting frog muscle fibres. *J. Physiol. (Lond.).* 481:689–708.

Chase, P. B., and M. J. Kushmerick. 1988. Effects of pH on contraction of rabbit fast and slow skeletal muscle fibers. *Biophys. J.* 53:935–946.

Chase, P. B., D. A. Martyn, M. J. Kushmerick, and A. M. Gordon. 1993. Effects of inorganic phosphate analogues on stiffness and unloaded shortening of skinned muscle fibres from rabbit. *J. Physiol. (Lond.).* 460:231–246.

Colomo, F., V. Lombardi, G. Menchetti, and G. Piazzesi. 1989a. The recovery of isometric tension after steady lengthening in tetanized fibres isolated from frog muscle. *J. Physiol. (Lond.).* 415:130P.

Colomo, F., V. Lombardi, and G. Piazzesi. 1989b. The recovery of tension in transients during steady lengthening of frog muscle fibres. *Pflügers Arch.* 414:245–247.

Colomo, F., V. Lombardi, and G. Piazzesi. 1988a. The mechanisms of force enhancement during constant velocity lengthening in tetanized single fibres of frog muscle. *Adv. Exp. Med. Biol.* 226:489–502.

Colomo, F., V. Lombardi, and G. Piazzesi. 1988b. The mechanisms of force enhancement during constant velocity lengthening in tetanized single fibres of frog muscle. *In* Molecular Mechanism of Muscle Contraction. H. Sugi and G. H. Pollack, editors. Plenum Press, New York.

Cooke, R., K. Franks, G. B. Luciani, and E. Pate. 1988. The inhibition of rabbit skeletal muscle contraction by hydrogen ions and phosphate. *J. Physiol. (Lond.).* 395:77–97.

Dantzig, J. A., and Y. E. Goldman. 1985. Suppression of muscle contraction by vanadate. *J. Gen. Physiol.* 86:305–327.

Edman, K. A. P., G. Elzinga, and M. I. M. Noble. 1978. Enhancement of mechanical performance by stretch during tetanic contractions of vertebrate skeletal muscle fibres. *J. Physiol. (Lond.).* 281:139–155.

Edman, K. A. P., G. Elzinga, and M. I. M. Noble. 1981. Critical sarcomere extension required to recruit a decaying component of extra force during stretch in tetanic contractions of frog skeletal muscle fibers. *J. Gen. Physiol.* 78:365–382.

Edman, K. A. P., G. Elzinga, and M. I. M. Noble. 1984. Stretch of contracting muscle fibres: evidence for regularly spaced active sites along the filaments and enhanced mechanical performance. *In* Contractile Mechanisms in Muscle, Vol. 170. G. H. Pollack and H. Sugi, editors. Plenum Press, New York. 739–751.

Edman, K. A. P., and T. Tsuchiya. 1996. Strain of passive elements during force enhancement by stretch in frog muscle fibres. *J. Physiol. (Lond.).* 490:191–205.

Eisenberg, E., T. L. Hill, and Y. Chen. 1980. Cross-bridge model of muscle contraction: quantitative analysis. *Biophys. J.* 29:195–227.

Flitney, F. W., and D. G. Hirst. 1978. Cross-bridge detachment and sarcomere "give" during stretch of active frog's muscle. *J. Physiol. (Lond.).* 276:449–465.

Godt, R. E., and D. W. Maughan. 1988. On the composition of the cytosol of relaxed skeletal muscle of the frog. *Am. J. Physiol.* 254:C591–C604.

Goldman, Y. E., and A. F. Huxley. 1994. Actin compliance: are you pulling my chain? *Biophys. J.* 67:2131–2136.

Goodno, C. C. 1982. Myosin active-site trapping with vanadate ion. *Methods Enzymol.* 85:116–123.

Gordon, A. M., R. E. Godt, S. K. B. Donaldson, and C. E. Harris. 1973. Tension in skinned frog muscle fibers in solutions of varying ionic strength and neutral salt composition. *J. Gen. Physiol.* 62:550–574.

Griffiths, P. J., K. Güth, H. J. Kuhn, J. C. Rüegg. 1980. Cross bridge slippage in skinned frog muscle fibres. *Biophys. Struct. Mech.* 7:107–124.

Güth, K., and H. J. Kuhn. 1978. Stiffness and tension during and after sudden length changes of glycerinated rabbit psoas muscle fibres. *Biophys. Struct. Mech.* 4:223–236.

Hamming, R. W. 1983. Digital Filters, 2nd Ed. Prentice-Hall, Englewood Cliffs, NJ. 120.

Harry, J. D., A. W. Ward, N. C. Heglund, D. L. Morgan, and T. A. McMahon. 1990. Cross-bridge cycling theories cannot explain high-speed lengthening behavior in frog muscle. *Biophys. J.* 57:201–208.

Hill, D. K. 1968. Tension due to interaction between the sliding filaments in resting striated muscle. The effect of stimulation. *J. Physiol. (Lond.).* 199:637–684.

Huxley, A. F. 1957. Muscle structure and theories of contraction. *Prog. Biophys.* 7:257–319.

Huxley, A. F., and R. M. Simmons. 1971. Proposed mechanism of force generation in striated muscle. *Nature.* 233:533–538.

Iwamoto, H. 1995. Strain sensitivity and turnover rate of low force cross-bridges in contracting skeletal muscle fibers in the presence of phosphate. *Biophys. J.* 68:243–250.

Lombardi, V., and G. Piazzesi. 1990. The contractile response during steady lengthening of stimulated frog muscle fibres. *J. Physiol. (Lond.).* 431:141–171.

Månsson, A. 1989. Changes in force and stiffness during stretch of skeletal muscle fibers, effects of hypertonicity. *Biophys. J.* 56:429–433.

Månsson, A. 1994. The tension response to stretch of intact skeletal muscle fibres of the frog at varied tonicity of the extracellular medium. *J. Muscle Res. Cell Motil.* 15:145–157.

Molloy, J. E., J. E. Burns, J. Kendrick-Jones, R. T. Tregear, and D. C. S. White. 1995. Movement and force produced by a single myosin head. *Nature.* 378:209–212.

Morgan, D. L. 1990. New insights into the behavior of muscle during active lengthening. *Biophys. J.* 57:209–221.

Morgan, D. L. 1994. An explanation for residual increased tension in striated muscle after stretch during contraction. *Exp. Physiol.* 79:831–838.

Pate, E., and R. Cooke. 1988. Energetics of the actomyosin bond in the filament array of muscle fibers. *Biophys. J.* 53:561–573.

Pate, E., and R. Cooke. 1989. A model for crossbridge action: the effects of ATP, ADP and P_i. *J. Muscle Res. Cell Motil.* 10:181–196.

Piazzesi, G., F. Francini, M. Linari, and V. Lombardi. 1992. Tension transients during steady lengthening of tetanized muscle fibres of the frog. *J. Physiol. (Lond.).* 445:659–711.

Piazzesi, G., M. Linari, and V. Lombardi. 1994. Kinetic requirements to simulate steady state and transient characteristics of contracting muscle. *Pluegers Arch.* 426:R178.55.

Piazzesi, G., and V. Lombardi. 1995. A cross-bridge model that is able to explain mechanical and energetic properties of shortening muscle. *Biophys. J.* 68:1966–1979.

Rayment, I., W. R. Rypniewski, K. Schmidt-Base, R. Smith, D. R. Tomchick, M. M. Benning, D. A. Winkelmann, G. Wesenberg, and H. M. Holden. 1993. Three-dimensional structure of myosin subfragment-1: a molecular motor. *Science.* 262:50–58.

Schoenberg, M. 1991. Equilibrium muscle cross-bridge behavior: theoretical considerations. *Biophys. J.* 60:679–689.

Seow, C. Y., and L. E. Ford. 1993. High ionic strength and low pH detain activated skinned rabbit skeletal muscle crossbridges in a low force state. *J. Gen. Physiol.* 101:487–511.

Stienen, G. J. M., P. G. A. Versteeg, Z. Papp, and G. Elzinga. 1992. Mechanical properties of skinned rabbit psoas and soleus muscle fibres during lengthening: effects of phosphate and Ca^{2+}. *J. Physiol. (Lond.).* 451:503–523.

Sugi, H. 1972. Tension changes during and after stretch in frog muscle fibres. *J. Physiol. (Lond.).* 225:237–253.

Tsuchiya, T., and H. Sugi. 1988. Muscle stiffness changes during enhancement and deficit of isometric force in response to slow length changes. *Adv. Exp. Med. Biol.* 226:503–511.

Zahalak, G. I. 1981. A distribution-moment approximation for kinetic theories of muscular contraction. *Math. Biosci.* 61:771–797.